

Analyses of Laser-Induced Periodic Surface Structures in Palladium Metal

Brandon Minor

June 7, 2013

Abstract

We used a femtosecond laser to create Laser-induced periodic surface structures, i.e. LIPSS, on samples of palladium for potential materials applications. LIPSS have been the subject of several interesting case studies involving the microstructuring and modification of materials. When shot with a short-pulse laser beam, a metal will bend and shape its surface according to the beams parameters, creating a periodic surface structure. We analyzed the results of femtosecond interaction with Palladium using a scanning electron microscope and MATLAB. The experimental parameters were fluence of the laser and number of shots on a particular spot. LIPSS were not produced with our chosen parameters, but other structures were created that could still be of use in experiments influenced by surface modification.

1 Background

1.1 LIPSS

Laser-induced periodic surface structures, i.e. LIPSS, are unique structures that only form under the influence of a femtosecond laser. A laser with a pulse on the order of femtoseconds transfers energy to a material fast enough to prevent the usual ablation of the surface, instead carving out sub-micron waves. LIPSS have been observed since the 1960s, but are still not thoroughly understood. For instance, in some transparent materials, periodic structures will actually form inside the material, rather than on the surface. Research has also uncovered ways to create structures with periodicities equal to, larger than, and much smaller than the wavelength λ of the laser, prompting the scientific community to investigate the origins of such vastly different wave patterns.

LIPSS are just not scientific curiosities; they also offer practical applications. Some studies have been focused on enhancing the tribological properties of a metal, i.e. the friction and wear experienced by it in a mechanical setting. One study [5] was actually able to produce and control the design of periodic structures on stainless steel using a femtosecond laser, providing greater tribological control. Others have been occupied with finding the perfect conditions for material ablation and structuring using different parameters on the femtosecond laser, looking for models that can apply to several types of metals. LIPSS could also be applied to battery material, where the patterning on the cathodes and anodes would result in a greater surface area. This project is applicable to all of these goals.

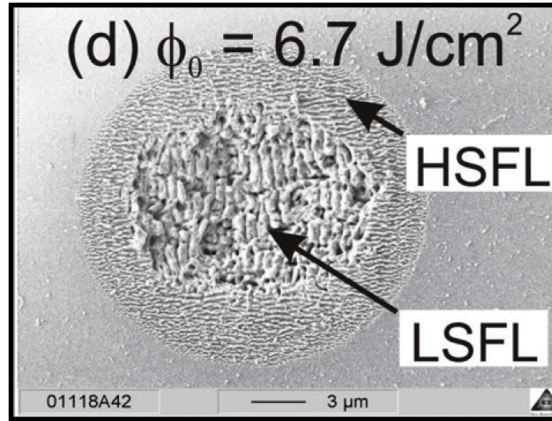


Figure 1: Example of LIPSS formation in silica.

The above figure shows a typical LIPSS result, displaying the surface of a silica sheet seen after a series of shots. Two structures appear: High Spatial Frequency LIPSS (HSFL) and Low Spatial Frequency LIPSS (LSFL). Second Harmonic Generation of the laser pulse frequency is responsible for the formation of HSFL. HSFL normally appear at a lower fluence than LSFL. In addition, increasing the number of pulses both makes the target area wider and produces more LSFL. The formula for the periodicity, either with HSFL or LSFL, is:

$$\Lambda = \frac{\lambda}{1 \pm \sin\theta}$$

The table below describes the parameters used in Figure 1 [2]. The fluences would be quite high if we were attempting regular ablation, but the ultrashort pulse of the femtosecond laser allows this amount of energy without much vaporization of the metal, giving us the LIPSS. The periodicities above the breakpoint are examples of HSFL; compared to the LSFL, they barely reach half the periodicity. Of course, one does not have to rely on periodicity to identify these structures if the direction of laser propagation is known: HSFL is always patterned perpendicular to the propagation of the laser beam.

Wavelength λ	Pulse length τ	N - single pulse sequences	Fluence ϕ (J/cm 2)	Periodicity of structure Λ (nm)
800nm	150fs	10	5	260
800nm	150fs	10	5.5	290
800nm	150fs	10	5.9	350
800nm	150fs	10	6.2	650
800nm	150fs	10	6.6	650
800nm	150fs	10	7.2	650
800nm	150fs	10	7.7	660
800nm	150fs	10	8.3	650
800nm	150fs	10	9	700
800nm	150fs	10	9.7	700

The next table focuses on the depth of the overall LIPSS structure into the surface [1]. The material tested was iridium phosphide, a semiconductor used in high-power applications. Iridium phosphide's ablation threshold is .23 J/cm 2 . However, you can see from the fluence column that all tests performed were at double that level, .58 J/cm 2 .

Wavelength λ	Pulse length τ	N - Single Pulse sequences	Fluence ϕ (J/cm ²)	Depth of pulse crater (nm)
800nm	130fs	1	0.58	55
800nm	130fs	2	0.58	130
800nm	130fs	3	0.58	180, jagged
800nm	130fs	4	0.58	200-250, very jagged

Not shown from this experiment is the period of the LIPSS themselves, though they give a very important result. As the number of shots N goes up, the spatial period of the LSFL goes down. In this case,

$$N = (2, 100) :: \Lambda = (750\text{nm}, 590\text{nm})$$

This is explained by the increasing angle of incidence on the crater. As the depth went down (around N=20), the Second Harmonic stopped affecting the metal. As a result, the HSFL disappeared, and the LSFL broadened out.

This data seems to back up the theory that LIPSS formation happens well above the ablation threshold; how far above dictates whether HSFL or LSFL are made, though after a certain number of shots, LSFL takes over the structure.

1.2 Scanning Electron Microscope

Scanning electron microscopes, or SEMs, are incredibly powerful research tools, allowing the study of objects not easily seen by even the strongest optical microscopes. Capable of reaching up to 500,000x magnification, SEMs represent a giant step forward in science, both through the technology implemented in its construction and the results obtained in its use.

1.2.1 Mechanics behind the SEM

SEMs work by rastering a focused electron beam over a small sample and collecting the resulting energy from the beam-target interactions. For this setup to work, there are three critical components: an electron source, lenses to focus the resulting electron beam, and sensors to gather particles from the sample. This electron source, also called an electron gun (which more accurately describes its properties), is held at the end of the vacuum chamber directly opposite the sample, and generally comes in two formats. Thermionic guns heat up a tungsten filament to emit their weakly-bound electrons. Field emission guns, the less common type, use an artificially produced magnetic field to pull electrons away from their host atoms in the gun. Both of these methods are capable of producing a strong enough stream of electrons to make the SEM function. The electrons move somewhat randomly away from the source, so there must be a way to focus the stream toward the sample.

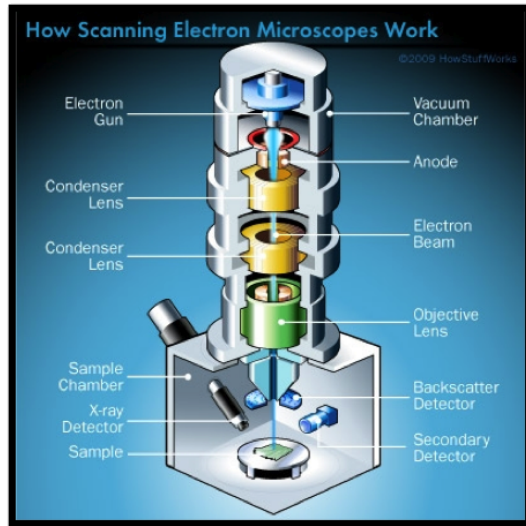


Figure 2: The anatomy of an SEM. The electron beam comes straight down into the sample, interacting with the sample to create different signals.

To better control the beam, a careful system of magnets (still referred to as lenses) is used. Just like the light from a bulb, an electron beam spreads out rapidly from its source. Condenser lenses are the strong magnets in the SEM that gather and refocus these beams towards the bottom of the chamber. Once the beam finally makes its way down (in nanoseconds), it is directed at the sample with adjustable magnetic deflection coils, a.k.a. the Objective Lens. It is these coils that control the magnification of the image; if a researcher wanted a larger magnification, they would increase the energy pumping through the source, creating more electrons, and program the magnetic coils to raster a smaller area of the sample. A slow raster will result in a sharper image, while a fast raster can make it easier to identify changes within a sample. It is actually this property of controlling magnification with magnets, rather than optics, which makes the SEM such a powerful instrument.

It is important to note that, as a large quantity of electrons are being shot at an object, the surface of the object will tend to charge up, resulting in a poor quality of image from electrostatic interference. Conductors, by definition holding no electric field and a constant potential, avoid this problem. If imaging an insulator, however, it may be necessary to sputter a small amount of a conductive metal, e.g. gold or copper, on its surface to increase the conductivity of the sample and the resolution on the SEM.



Figure 3: A spider sputter-coated in gold, in preparation for SEM imaging.

One can also tilt the sample stage one way or another to neutralize the electromagnetic effects. The beam backscatter can be very localized, to the point that excess electrons build up too quickly to dissipate. Tilting the stage around its x-axis can ricochet the electrons down and away from the rest of the sample, preventing this buildup.

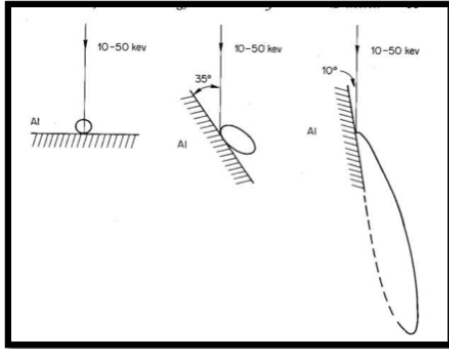


Figure 4: A graphical representation of the tilt concept. The loop's area depicts how many electrons escape the pull of the sample surface.

1.2.2 Imaging

Striking a conducting sample with a strong electron beam will result in several things at once:

- Backscattered Electrons** - Similar to the ricochet of billiard balls against one another, backscatter electrons are electrons from the main electron stream that are knocked back from the surface of the sample. A ring of sensors specifically designed to pick up backscatter are usually positioned directly above the sample.
- Secondary Electrons** - These are low-energy electrons produced in the surface of a sample, under 50eV. In contrast to backscattered electrons, which can come from deep within a sample, secondary electrons only have enough energy to break free if they don't have much blocking their path, i.e. close to the surface. Hence, gathering secondary electrons gives a researcher an incredibly crisp picture of the topography, or surface textures, of a sample. Secondary Electron sensors (as well as their Backscatter counterparts) produce monochromatic images; due to the nature of the data collection, there is not enough information about the source of the gathered electron to assign any sort of color. However, this problem can be circumvented with other methods, mainly cathodoluminescence or x-ray analysis.
- X-ray Analysis** - As energetic electrons interact with the sample surface, the removal of an electron from a core orbital leads to the formation of x-rays, which are then picked up by a spectrometer. Each x-ray energy correlates to a specific element. The SEM uses this to produce composition information. Unlike backscatter electrons, x-ray signals are not the result of free electrons, but rather energy changes within the substance itself.
- Cathodoluminescence** - X-rays are not the only wavelengths produced when a sample is hit; IR, UV, and visible result as well, collectively referred to as cathodoluminescent waves. As the name might suggest, this mode aids in coloring the sample image. Sensors specifically designed to pick up these waves sort and analyze scan by scan to return a colored image.

1.2.3 The Advantages of SEM, and use for LIPSS

When looking for small things on a complicated structure, there are only so many options a researcher can choose. TEMs, or transmission electron microscopes, utilize the complete transmission of individual electrons through an ultrathin sample, making imaging on the order of Angstroms possible. However, TEMs have a very narrow field of view; a typical stage is no bigger than 2 mm wide. SEMs allow for a larger field, and its secondary electron sensors give a depth of focus to topographic images that TEMs cannot deliver without slicing through a sample multiple times.

Compared to optical microscopes, SEMs seem to have an advantage in almost every respect, at least technologically. However, even high-powered optical microscopes do not require the care that a SEM does. If the vacuum chamber of a SEM leaks anywhere, or any probes break, or any sensors malfunction, the microscope is essentially unusable. Most replacement parts for a SEM reach well into the thousands of dollars, and several hours of training are needed if one wants to avoid ramming the stage against a sensor. If nanometer-wide images of an object are not essential to the study, an optical microscope will probably save a researcher both time and effort.

For our purposes, the SEM was perfect. LIPSS form on the order of 10^{-6} m, so it would be physically impossible to see the results of the test with anything weaker, much less analyze parameters. With the image capture allowed by the SEM, we could hone in on the exact section of the sample that we needed, and save the image for later use. This high quality production was what made this discussion possible.

2 Experimental Setup

2.1 Materials

Palladium metal was chosen as our test metal, as it served a dual purpose. In addition to the fact that we could find no record of LIPSS parametrization of palladium, my advisors and I were also interested in the effects of LIPSS on the effectiveness of deuterium loading. Such loading is interesting in its own right, but gained notoriety in the Pons-Fleischmann experiments, where it was used to reportedly demonstrate cold fusion. This report does not treat these speculated effects. The foils that we used were 1 mm thick.

As LIPSS only forms with the use of a femtosecond pulse, we processed the palladium foils with a PHAROS (Light Conversion, Ltd.) laser system. The PHAROS produces laser pulses with 90-200 fs duration, and has a center wavelength of 1028 nm. The pulse energy of the beam can go as high as $30 \mu\text{J}$. In our experiments, the Gaussian spot size was $10\mu\text{m}$. The combination of power and shot size allowed us to produce fluences up to 5 J/cm^2 , the maximum level used for our tests.

2.2 Parameters

All tests were done on the same strip of palladium foil, to assure consistent conditions for every test. We employed five fluences and five laser pulse numbers on a given spot, resulting in 25 different irradiated combinations. The design of the experiment required that each combination be in its own space, so the palladium was sectioned off appropriately:

	Control	.5 (5x shot)	2 J/cm^2	3 J/cm^2	4 J/cm^2	5 J/cm^2
100	
75					
50	
25	
1	

Figure 5: Experimental setup.

The left-most column in Figure 5 designates the number of shots per row; since the available literature indicates that more LSFL form as more shots are fired. We set the upper shot bound to a high number in order to test that effect in palladium. The five columns with shots in them are labeled with their corresponding fluences. We used an XY translation stage and an EO modulator to create the raster pattern within the pre-programmed range, a square 5 mm on each side. The setup was programmed using G-Code. The EO modulator allowed us to change the fluence quickly in order to complete the whole sample irradiation with one program. Fluence ranged from $0.5 - 5 \text{ J/cm}^2$.

N.B. - Due to a programming error, the first test (0.5 J/cm^2) was run without translation of the stage in the X-direction; this is designated as a (5x) in Figure 5 above. However, this mistake was not a disaster; rather, it allowed us to analyze the effect of each shot count times 5, resulting in a top shot count per area of 500. All references to 0.5 J/cm^2 correspond to this 5x-over test.

3 Results and Qualitative Analysis

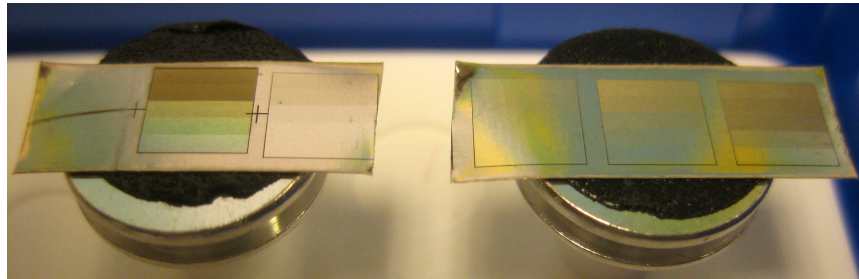


Figure 6: The palladium strip, post-processing and cut in two for easier mounting on the SEM sample holders. The orientation of the tests is comparable to Figure 5. Notice that the 0.5 J/cm^2 column on the center of the left sample is much darker than its neighbors due to the flawed program used to raster the laser.

The results of the experiment are shown above. The layers of shots can be clearly seen from the reflection of the light. More shots per pass meant a 'darker' layer. To get high magnification images of the LIPSS that formed, we took the samples to the SEM. The palladium strip was too long to place on the SEM's stage without modification, so it was split into two parts.

Due to the time constraints imposed when using the SEM, we were only able to capture images of the 0.5, 3, and 5 J/cm² sections of the palladium. Images were captured so that data from two shot counts appeared in a single image. Images of a given section were generally captured at two different magnification levels.

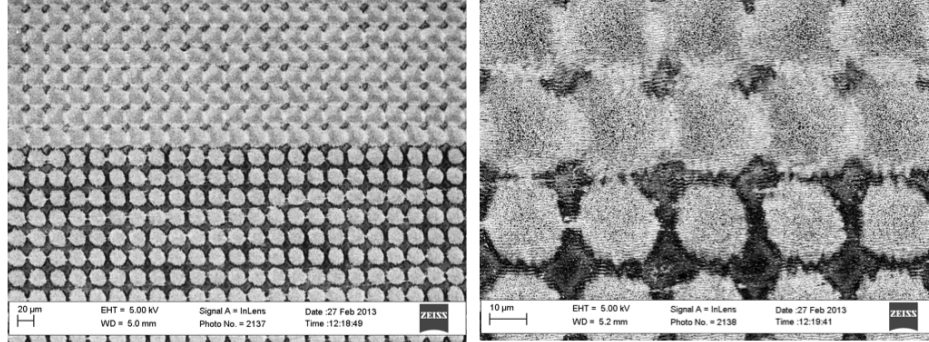


Figure 7: An example of an SEM image: the 0.5 J/cm² test, two different shot counts at two magnifications.

Qualitatively, there is much to be gained in the images. There are what appear to be wave-like structures in the middle of each dot. Dots expanded in area as more shots were fired, an effect demonstrated in Figure 7. This agrees well with the literature on LIPSS: more shots results in a wider LSFL pattern.

Though most areas shot did create patterns of some kind (as they were not yet determined to be LIPSS), some shots with many repetitions ceased to create a wave pattern and instead started to form a sponge-like surface with seemingly no pattern. In between these 'sponges', there were what seemed to be LSFL patterns. This seems to indicate that the mesh structures were the result of too many shots, too strong a fluence for the metal, or a combination of the two. However, it is important to note that the metal was not ablated, as the mesh was only slightly concave (this could be deduced by the accurate focus of the SEM). Despite this appearance, meshed sections were still analyzed for possible oscillation patterns.

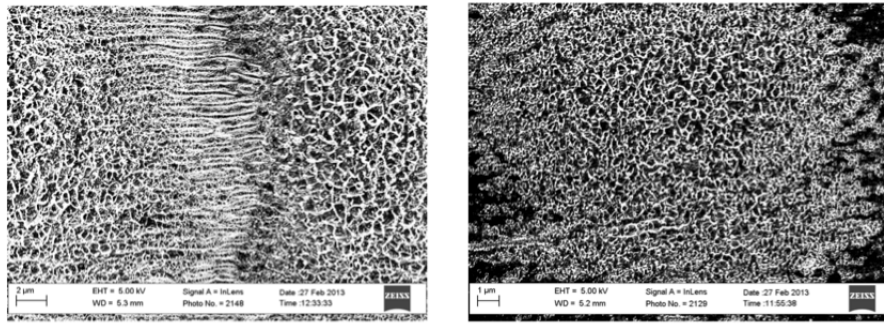


Figure 8: Sponge-like structures on the surface of the palladium. Left picture: 0.5 J/cm². Right: 3 J/cm².

Other sections of the foil did not have any markings. The left picture of Figure 9 is a macroscopic image of an non-irradiated section on the foil, resting between two tested fluence levels. Upon closer inspection of some of these rows, large sections of untouched palladium

can be seen within. This is the case with the 5 J/cm^2 rows shot once. It seems that one pulse did not transfer enough energy to the metal for noticeable structures to form. Nor is the dot uniform; though there was clearly some effect, the Gaussian beam's focus did not translate to an even dispersion of energy on the bare metal. Less obvious examples of this effect can be seen in Figure 7: with more shots per area, the dots tended to increase in width more than height.

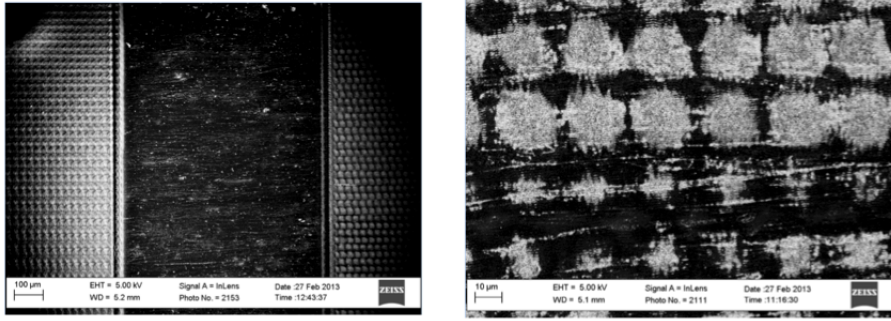


Figure 9: Comparing bare palladium metal (left) with irradiated metal with weak patterns (5 J/cm^2 , 1-shot to 20-shot)

One more detail can be gleaned at nanometer scale. Inside the sponge structures (see Fig. 8), small orbs of palladium could be seen. This is a strong indication of melting. In theory, a femtosecond laser's pulse should be so fast that there is very little heat transfer. However, these orbs were only found in the areas with high shot number; Figure 10 had 500 shots, and though it was at a very low fluence, there was still enough repetition to exhibit heating. Melting the palladium, whether through high shot repetition or high fluence, could very well destroy the LIPSS.

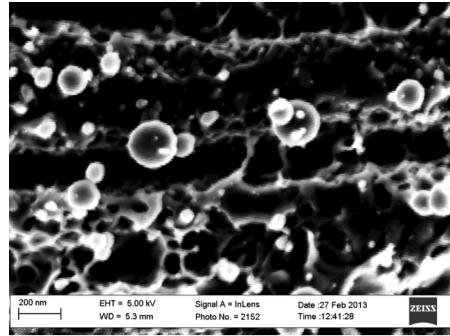


Figure 10: A nanoscale image of the lasered palladium. 0.5 J/cm^2 , 100-shot. Orbs of melted metal are suspended throughout.

4 Parameterization and Discussion

LIPSS are defined by their periodicity; thus, we analyzed each SEM image for any strong wave patterns. This analysis was done in MATLAB. MATLAB processes images as a matrix according to brightness. Since the SEM assigns images with brightness variations dependent

on local typography, analyzing a band of waves became as simple as plotting the values of apparent brightness over a certain range. The resulting graph would be an accurate representation of the (scaled) amplitude and frequency of the waves.

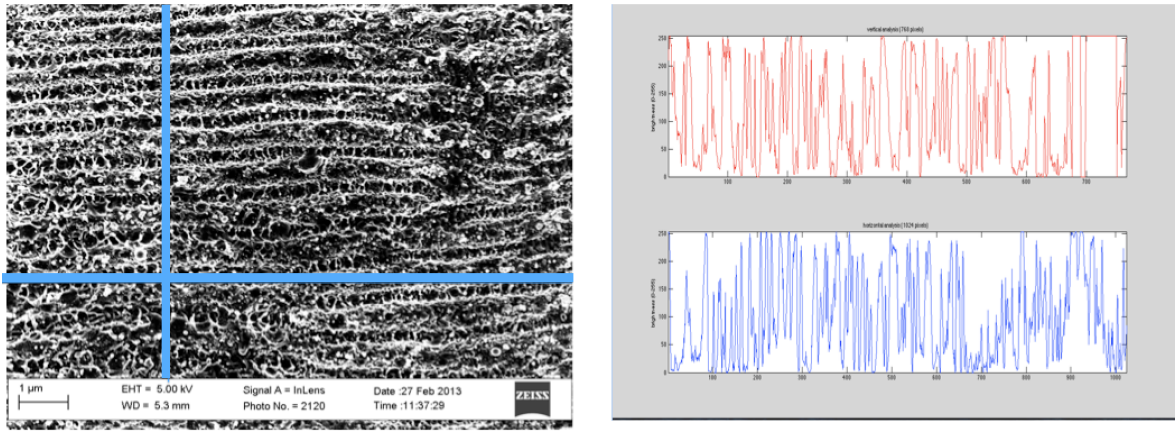


Figure 11: Analysis of the wave structure through MATLAB, pre-transform.

All pictures were 1024x768 pixels, so if a signal was close to the width of a pixel in frequency, it would be harder to detect. For this reason, we used the highest magnification of a structure that we had for analysis. Often, this was on the scale of 100 pixels per micron.

MATLAB's Fast Fourier Transform method was used as an efficient way to find the most common periodicity in a brightness plot. The reason for this was two-fold: if there was any periodicity, there would have been a strong peak somewhere in the FFT, and secondly, this peak would give us the periodicity of the LIPSS. Thus, in one operation, both faulty and valuable features could be discerned.

Fourier transforms were produced for a total of 8 photos in the 0.5 J/cm^2 range, 7 in the 3 J/cm^2 range, and 8 in the 5 J/cm^2 range. As indicated in Figure 11, multiple vertical and horizontal scans were produced for each photo. Before a Fourier Transfer was actually produced, the data were put through a smoothing function to highlight any periodicity that might have been blurred out by noise in the data. Figure 12 shows this result; though the brightness data are noticeably different, the FFT was not drastically affected.

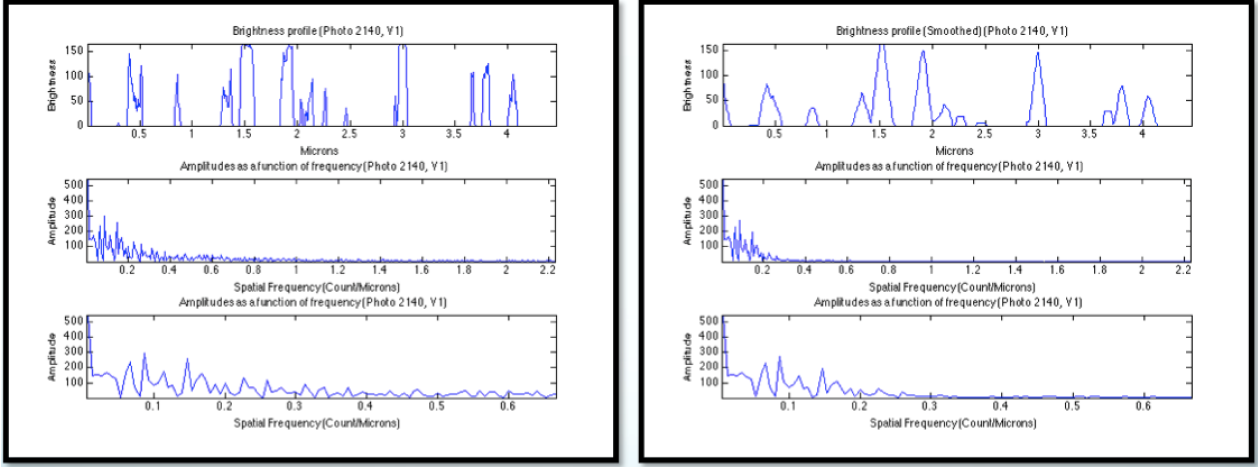


Figure 12: Fourier Transforms created from both original (left) and smoothed (right) brightness data. The top plot represents the brightness; the middle is the full FFT plot; the bottom is a zoom-in on the lower half of the FFT's x-axis, done to accentuate the low frequencies picked up.

After all brightness samples were put through the FFT, we sampled the most frequent periodicity from each sample (found by finding the maximum peak on the FFT). Each of these was plotted individually, with different fluences on different plots. Figure 13 displays these results for .5, 3, and 5 J/cm².

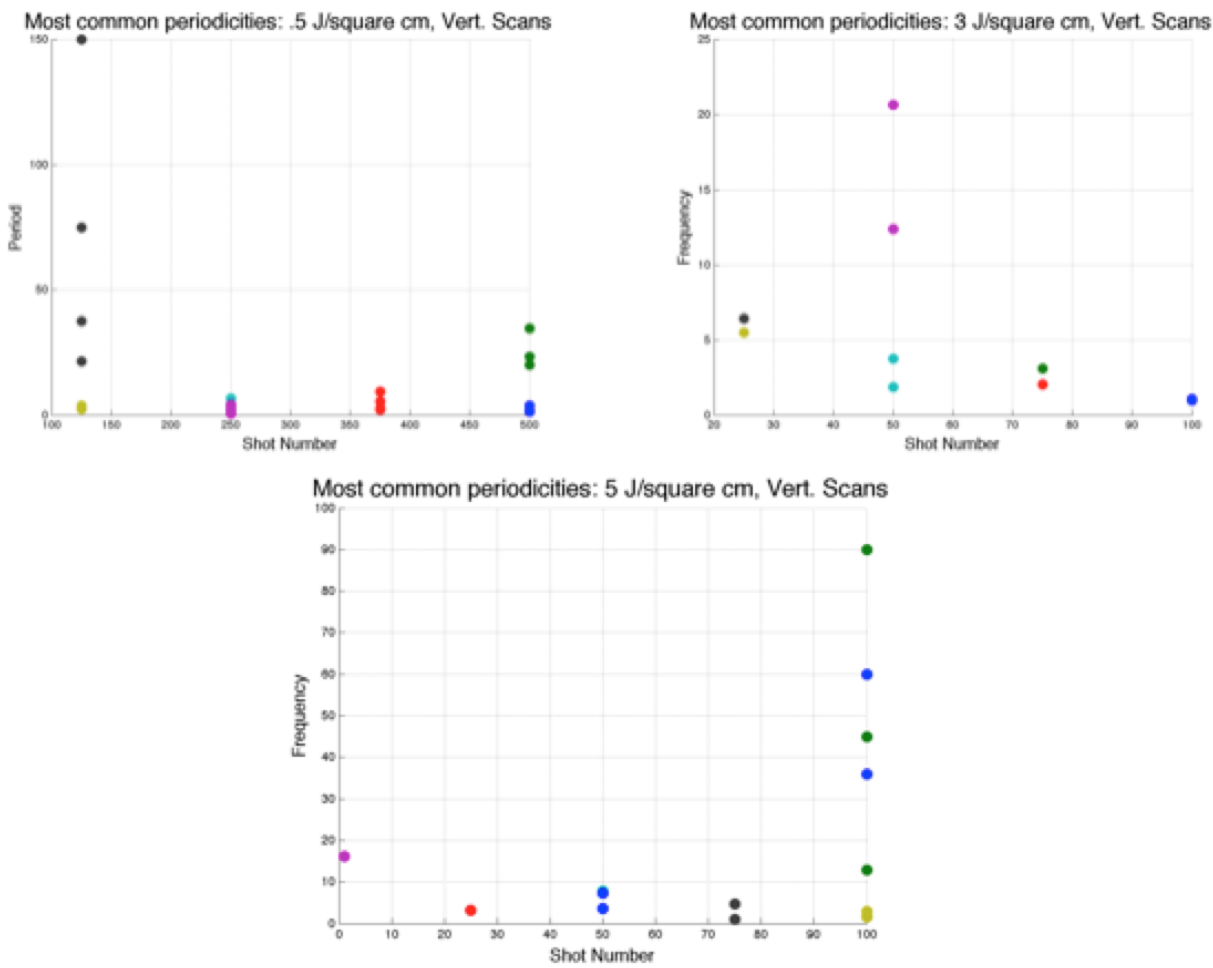


Figure 13: Most common periodicities in three fluence sets.

Literature available on LIPSS indicates that as the fluence of a shot increases, the periodicity of the wave should increase as well (See Figure 14 below). This is not the case in our Palladium samples. Comparing all three graphs shows a scatter between fluence and shot level that does not produce a linear or exponential trend. Generally, LIPSS should also increase in periodicity as the shot number increases, but no such trend is visible.

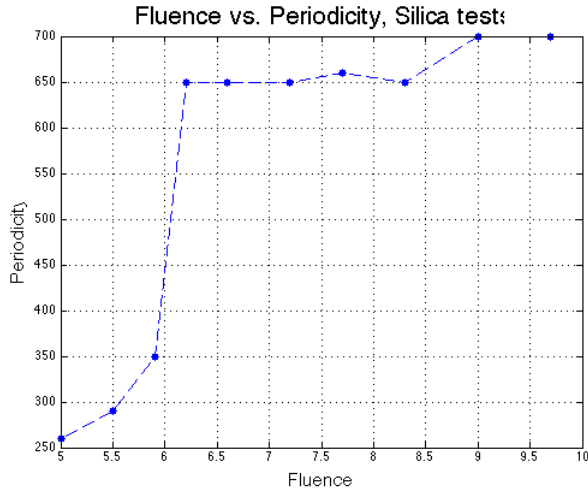


Figure 14: Fluence vs. Periodicity plot, based off of results from Table 1 on Page 2

5 Conclusion

It can be said with a high degree of certainty that LIPSS were not found at a low fluence. What's less certain is what occurred at higher energy. There's a vague upward trend in the 5 J/cm^2 plot of Figure 12 that might indicate that something was occurring. However, the condition of these tests prevent knowing anything for sure. This result, with the promise of possible LIPSS, prompts several improvements:

1. Spread the shots farther apart: As could be seen in many of the photos taken, the only wave-like structures that could be discerned were between shots. I believe that as more shots were fired, whatever structure was produced spread in diameter; by the time 25, 50, or 100 shots were fired, there was so much interference that it was impossible to tell what wave came from what. Having less shots per row would be an easy fix here.
2. Start at a higher fluence: Across the board, more waves were produced at higher fluences than lower ones. These weren't necessarily LIPSS, but this observation is in agreement with available LIPSS literature. For instance, the experiment that produced Figure 1 dealt with Silica as its medium. Silica has a known ablation threshold of 2.4 J/cm^2 ; tests that produced LIPSS started at 5 J/cm^2 , more than twice that fluence. This higher-than-threshold fluence might be a necessary component to LIPSS formation, and something that we overlooked during experimental design. Given that the PHAROS laser system that we used has a peak fluence of 30 J/cm^2 , there's plenty of potential to crank up the energy.
3. Investigate meshed structures: though there was no real way to tell what parameter was most responsible for the creation of the mesh-like structures in each shot, their origin should be investigated, if only to learn how to avoid their occurrence in future tests. It might be the case that the improvements above will eliminate them altogether, but we don't know this for certain. The next round of tests should categorize under what conditions these meshes are created.

Sadly, our original parameterization experiment could not come to fruition; due to results that we did not anticipate, we could not produce LIPSS of any kind. That being said, the things learned through these experiments have put us in a great position for a new set of tests, as the above improvements suggest.

6 Acknowledgements

Thanks to Prof. Gerald Feldman for pulling me into Physics in the first place. I am sure that it can be a bit tiring working with a think-for-yourselfer all of the time, but he does a good job putting up with it all, and that's something that I would not have found anywhere else.

For his help in inspiring this research and taking up the experiment where I could not, I would like to thank Prof. Scott Mathews of Catholic University. He made this experiment possible, and gave the research a purpose.

For contributing his expertise and connections, as well as enthusiasm for the subject, I would like to thank Prof. David Nagel of George Washington University. I would have nothing to analyze without his help at the SEM, and would have wasted quite a bit of time without his guidance. Thanks to the SEAS department for loaning the SEM to this study.

I would like to thank the Materials Science Section of the Naval Reserach Laboratory and their Director, Alberto Pique, for their generosity in lending their time and materials to this experiment.

7 References

- 1 Bonse, Munz, and Sturm, Structure formation on the surface of indium phosphide irradiated by femtosecond laser pulses. *J. Appl. Phys.* 97, 013538 (2005)
- 2 Hohm et al., Femtosecond laser-induced periodic surface structures on silica. *J. Appl. Phys.* 112, 014901 (2012)
- 3 J. Z. P. Skolski, Inhomogeneous absorption of laser radiation: Trigger of LIPSS formation, Proceedings of the 13th International Symposium on Laser Precision Microfabrication, June 12-15, 2012, The Catholic University of America, Washington, DC USA, Paper # 33
- 4 Miyazaki, Kenzo and Miyaji, Godai, Periodic Nanopattern Formation on Si with Femtosecond-Laser-induced Surface Plasmon Polaritons, Proceedings of the 13th International Symposium on Laser Precision Microfabrication, June 12-15, 2012, The Catholic University of America, Washington, DC USA, Paper #35
- 5 Naoki Yasumaru et al., Femtosecond-laser-induced nanostructure formed on stainless steel, Proceedings of the 13th International Symposium on Laser Precision Microfabrication, June 12-15, 2012, The Catholic University of America, Washington, DC USA, Paper 14

- 6 Robbins, Roger. Scanning Electron microscope Operation. Dallas, TX: The University of Texas at Dallas, 2011. Web. 21 Sept. 2012.
<http://www.utdallas.edu/rar011300/SEM/Scanning%20Electron%20Microscope%20Operation.pdf>.
- 7 S. Y. Wang, Femtosecond laser induced surface nanostructures on copper, Proceedings of the 13th International Symposium on Laser Precision Microfabrication, June 12-15, 2012, The Catholic University of America, Washington, DC USA, Paper #10
- 8 Transmission Electron Microscopy. Wikipedia, n.d. Web. 21 Sept. 2012.
http://en.wikipedia.org/wiki/Transmission_electron_microscopy